NJC

LETTER

View Article Online
View Journal | View Issue

Cite this: *New J. Chem.*, 2019, 43, 17927

Received 10th September 2019,
Accepted 25th October 2019

DOI: 10.1039/c9nj04659c

rsc.li/njc

A dry chemical method for dispersing Ir nanoparticles in the pores of activated carbon and their X-ray absorption spectroscopy analysis†

Hiroyuki Itoi, *[a] Takashi Tachikawa,[b] Ryutaro Suzuki,[a] Hideyuki Hasegawa,[a] Hiroyuki Iwata,[c] Yoshimi Ohzawa,[a] Atsushi Beniya[b] and Shougo Higashi *[b]

Ir nanoparticles are finely dispersed over whole particles of activated carbon (AC) *via* the gas phase adsorption of an organoiridium complex in the AC and subsequent heat treatment. Structural analysis of the supported Ir is performed in combination with X-ray absorption spectroscopy.

Metal nanoparticles have been widely studied for their use in catalysts, electronics, sensors, and many other fields. In particular, precious metals, such as platinum, iridium, and rhodium, have high catalytic activity and selectivity and have been used in industry for catalytic applications. The amount used can be easily reduced by decreasing the size of the metal nanoparticles, which increases their active surface areas per unit mass. Moreover, decreasing the particle size demonstrates an enhancement of the catalytic activity per unit surface area of the metals.[1–3] The resulting synergetic effect, which is also affected by the kind of support, has been of significant interest.[4]

For catalyst applications, metal nanoparticles are generally deposited or grown on thermally and mechanically stable metal oxides (*e.g.*, silica and alumina), which serve as catalyst supports. Normally, supported metal nanoparticles are prepared *via* a wet chemical method using relatively inexpensive inorganic metal complexes compared to organometallic complexes, whereby an inorganic metal complex is mixed with a support in the liquid phase and reduced with a reducing reagent. In addition to metal oxide supports, carbon-based materials, such as carbon black, have also been used as catalyst supports, due to their high electrical conductivity and chemical stability. As a result, fuel cell catalysts using carbon-based supports have undergone intense study to demonstrate their early practical applications.[5–7] Carbon materials have versatile structures, which include fullerenes,[8] carbon nanotubes,[9,10] graphenes,[11] *etc.* In addition to these nanostructured carbons, activated carbon (AC) has a large surface area and a strong adsorption property, and its surface area and pore size can be precisely controlled by appropriate synthetic methods and conditions. Such nanosized pore spaces confine the materials adsorbed or synthesized in the pores, and thus can be used as a template for synthesizing polymers[12–16] or nanoparticles[17,18] inside them.

Here, we demonstrate the fine dispersion of Ir nanoparticles over AC using an organoiridium complex and perform their structural analysis using X-ray absorption spectroscopy. In comparison to inorganic metal complexes, organometallic complexes have relatively high vapor pressure and can be reduced just through heat treatment, without requiring reducing reagents or gases.[19,20] For the preparation of the AC-supported Ir nanoparticles, we examine the gas phase adsorption of an organoiridium complex in AC to synthesize AC/organoiridium complex hybrids and their subsequent heat treatment (*i.e.*, a dry chemical method). This method does not need any special apparatus, organic solvents, cumbersome chemical reactions, or the synthesis of nanostructured carbons *via* a multi-step process. Although any porous carbon can be used in this method, the superiority of this method is the availability of AC, which is commercially available at high volumes. The advantage of this method over a wet chemical method is the controllability of the accurate weight ratios of the AC and organometallic complex in the AC/organometallic complex hybrids, unless the amount of an organometallic complex exceeds the saturation amount of the AC used.[15,21,22] The accurate adjustment of the weight ratio enables reproducible dispersion of Ir nanoparticles with the aid of the pore confinement of the AC, which controls the size of the Ir nanoparticles to below the pore size of the AC used. Our strategy establishes the methodology for systematically and reproducibly synthesizing metal nanoparticles without the formation of undesired large nanoparticles on porous carbons. We believe that our method facilitates the optimization of the size of nanoparticles for the synthetic catalysts and electrocatalysts.

[a] *Department of Applied Chemistry, Aichi Institute of Technology, Yachigusa 1247, Yakusa-cho, Toyota 470-0392, Japan. E-mail: itoi-hiroyuki@aitech.ac.jp*
[b] *Frontier Research-Domain, Toyota Central R&D Labs, Inc., Yokomichi 41-1, Nagakute, 480-1192, Japan. E-mail: shigashi@mosk.tytlabs.co.jp*
[c] *Department of Electrical and Electronics Engineering, Aichi Institute of Technology, Yachigusa 1247, Yakusa-cho, Toyota 470-0392, Japan*

† Electronic supplementary information (ESI) available. See DOI: 10.1039/c9nj04659c

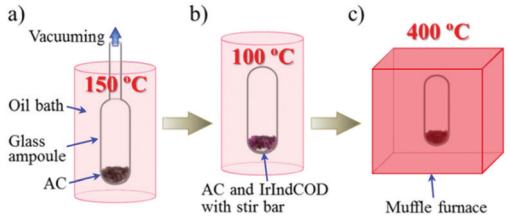

Fig. 1 Schematic of the sample preparation. (a) Vacuum drying of AC at 150 °C. (b) Adsorption of IrIndCOD in AC at 100 °C with stirring. (c) Heat treatment at 400 °C.

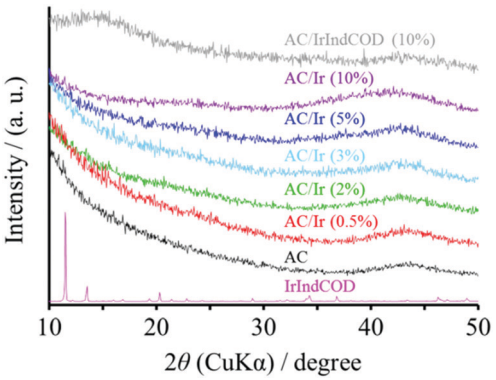

Fig. 2 XRD patterns of AC, IrIndCOD, AC/IrIndCOD (10%), and the AC/Ir samples.

Fig. 1 illustrates an experimental schematic of the gas phase adsorption of an Ir complex, (1,5-cyclooctadiene)-η^5-indenyl iridium(I) (IrIndCOD), in activated carbon (AC) and its subsequent thermal decomposition. The AC used in this study is KOH-activated carbon with a surface area of 3160 $m^2\ g^{-1}$ and pore sizes less than 4 nm (Fig. S1, ESI†). AC was dried under vacuum using a glass ampoule (Fig. 1a), and the amount of dried AC was determined by the weight difference between the empty ampoule and the one containing the dried AC. IrIndCOD was precisely weighed to create accurate AC/Ir weight ratios of $(100 - X):X$ (X = 0.5–10), and added to the ampoule with a magnetic stir bar, followed by sealing the ampoule under vacuum. The ampoule was then heated at a ramp rate of 1 °C min^{-1} up to 100 °C and kept at this temperature for 24 h with stirring to adsorb IrIndCOD uniformly over the entirety of the AC particles (Fig. 1b). Because IrIndCOD crystals are larger than the pore size of AC, vaporized IrIndCOD molecules may be adsorbed in the AC pores preferentially in the vicinity of the IrIndCOD crystals unless the mixture of AC and IrIndCOD is stirred. The decomposition of adsorbed IrIndCOD in the resulting AC/IrIndCOD samples was caused by heating the ampoule at 400 °C for 3 h (Fig. 1c). The resulting samples are denoted AC/Ir (X%).

Fig. 2 shows the X-ray diffraction (XRD) patterns of IrIndCOD, AC, and the AC/Ir samples. In addition, the XRD pattern of AC/IrIndCOD (10%), which is the precursor of AC/Ir (10%) and has the maximum Ir content among all the AC/Ir precursors, is also plotted for comparison. As shown in the figure, AC shows a carbon (10) diffraction at 44°, but does not show a carbon (002) diffraction at *ca.* 26° because the carbon structure is highly activated by KOH and few stacked graphene sheets remain.[23] Meanwhile, IrIndCOD shows many distinct peaks derived from its crystalline structure. Although the weight percent of IrIndCOD in AC/IrIndCOD (10%) is as high as 19 wt%, the sample does not show any distinct peaks of IrIndCOD. Instead, AC/IrIndCOD (10%) shows a broad peak at *ca.* 15° because IrIndCOD is adsorbed inside the nanosized pores of AC and does not form sufficiently crystalline structures in such constrained spaces to display distinct peaks;[21,22] *i.e.*, IrIndCOD exists in an amorphous phase in the AC pores. It has been reported that the amorphous phases of adsorbed metallocenes (*e.g.*, ferrocene and cobaltocene) in the constrained spaces of carbon nanotubes (CNTs) can be identified by transmittance electron microscopy (TEM) imaging.[24,25] This observation was realized due to the fact that the highly crystalline structures of CNTs made it possible to distinguish the amorphous metallocenes from the highly crystalline CNT wall. If IrIndCOD is not completely adsorbed in the AC pores, the sample should show distinct peaks originating from the remaining IrIndCOD crystals on the AC particles. Therefore, the IrIndCOD in AC/IrIndCOD (10%) is finely dispersed inside the AC pores, suggesting that IrIndCOD is completely adsorbed for the other AC/Ir precursors (*i.e.*, the AC/IrIndCOD samples). On the other hand, the AC/Ir samples do not visibly show the broad peak at 15° in their XRD patterns, suggesting the decomposition of IrIndCOD during the heat treatment at 400 °C. Nevertheless, the AC/Ir samples also do not show any distinct peaks derived from the face-centered cubic (fcc) structure of the Ir nanoparticles,[26] even for AC/Ir (10%) with the highest Ir loading among all the AC/Ir samples. These results suggest that the AC/Ir samples contain small Ir nanoparticles. However, there remain undecomposed IrIndCOD structures, and the size of the Ir nanoparticles cannot be estimated from such a broad peak in their XRD patterns. These issues are discussed in the following sections.

The TEM images of AC, AC/IrIndCOD (10%), AC/Ir (0.5%), and AC/Ir (10%) are shown in Fig. 3. Since the IrIndCOD in AC/IrIndCOD (10%) is finely dispersed inside the amorphous AC pores, no difference was observed between AC and AC/IrIndCOD (10%) (Fig. 3a and b), *i.e.*, the IrIndCOD is adsorbed as a complex without decomposition. In contrast, nanoparticles are observed in AC/Ir (0.5%) and AC/Ir (10%) (Fig. 3c and d). Although the Ir content largely differs depending on the samples, the size of the Ir nanoparticles is controlled to below *ca.* 4 nm due to the pore confinement effect of the AC, of which the maximum pore size is *ca.* 4 nm (Fig. S1, ESI†). AC/Ir (10%) contains a large amount of Ir, but we confirmed very fine dispersion of Ir nanoparticles over the whole AC particles. By considering the least Ir loading in AC/Ir (0.5%) among all the AC/Ir samples, the amount of the observed Ir nanoparticles in Fig. 3c is relatively large, because the Ir nanoparticles in AC/Ir (0.5%) exist preferentially near the particle surface of AC, which was further confirmed from the TEM and X-ray photoelectron spectroscopy analyses (for details, see the ESI†). We have previously reported the dispersion of Ni subnanoclusters on zeolite-templated carbon (ZTC) *via* a dry chemical method.[27] ZTC is prepared using zeolite as a template and has a

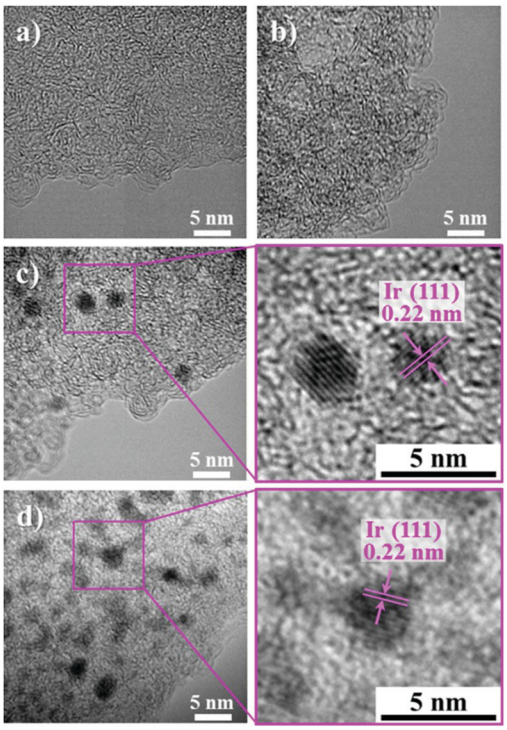

Fig. 3 TEM images of (a) AC, (b) AC/IrIndCOD (10%), (c) AC/Ir (0.5%), and (d) AC/Ir (10%).

uniform pore size of 1.2 nm.[28] However, in addition to the subnanoclusters, nanoparticles larger than the pore size of ZTC also form on the particle surface of ZTC. The undesired formation of the large nanoparticles, which hampers the rigorous study of the size-dependent performances of nanoparticles, is considered to proceed during the adsorption procedure. In the previous method, an organonickel complex was separated from ZTC in a glass ampoule during the adsorption, and decomposed on the ZTC particles before adsorption. In the present study, we modified the adsorption method by directly mixing IrIndCOD and AC with stirring and gradually increasing the temperature so that IrIndCOD can be completely adsorbed in the pores of AC without decomposition. AC/Ir (0.5%) contains the smallest amount of Ir among all the AC/Ir samples, but the maximum size of the Ir nanoparticles is almost the same as that in AC/Ir (10%). This result implies that Ir atoms resulting from the thermally decomposed IrIndCOD rapidly diffuse inside the AC pores to grow into nanoparticles during the heat treatment. However, the TEM observation and XRD analysis cannot conclude that all the adsorbed IrIndCOD molecules were completely decomposed by the heat treatment.

Fig. 4 shows the X-ray absorption near edge structure (XANES) spectra of the Ir L_3 edge for the AC/Ir samples. The XANES spectra of Ir, IrIndCOD, and IrO_2 are also shown in the figure. The spectrum shapes of the AC/Ir samples do not match with either that of individual Ir, IrO_2, and IrIndCOD spectra, so it is natural to think that those obtained spectra are the mixture of the individual spectra of Ir, IrO_2, and IrIndCOD. Thus, we tried to fit the obtained XANES spectra by linearly combining the individual Ir, IrO_2, and IrIndCOD spectra. The spectra were successfully fitted well with the parameters as summarized in Table 1. We determined the spectrum agreement using *R*-factors.[29–31] Note that the ratios used for the linear combination fitting are equal to the molar ratios (for details, see the ESI†). In the TEM analysis, the formation of Ir nanoparticles was confirmed, but no IrO_2 was detected; however our XANES analyses revealed the existence of IrO_2 in all five samples due to the oxidation of the outer surfaces of the Ir nanoparticles. The reason why clear evidence of IrO_2 was absent in the XRD patterns for the AC/Ir samples is explained by the very thin IrO_2 layers formed on the outer surface of the Ir nanoparticles. Since the sizes of the Ir nanoparticles were controlled below the pore sizes of AC, it was difficult to detect such very thin IrO_2 layers clearly with our laboratory XRD instrument. Meanwhile, the content of IrIndCOD is low compared to those of Ir and IrO_2 for all the samples, but we see a tendency for it to decrease with decreasing IrIndCOD precursor loading. A good *R*-factor of 0.004 in the linear fitting was achieved for the simulated spectrum of AC/Ir (0.5%) (*i.e.*, the minimum IrIndCOD loaded sample), based on the assumption that IrIndCOD was completely decomposed, suggesting that the content of IrIndCOD was negligible (Fig. S2, ESI†). However, the results obtained from the XANES spectra revealed that the other AC/Ir samples contain undecomposed IrIndCOD.

In practical applications, the challenge is to reduce the amount of undecomposed metal precursors and maximize the nanoparticle yield with controlled sizes. There are two options for this purpose: increasing the temperature and/or the duration of the heat treatment, both of which help the decomposition of the remaining IrIndCOD. In fact, we confirmed an increase in

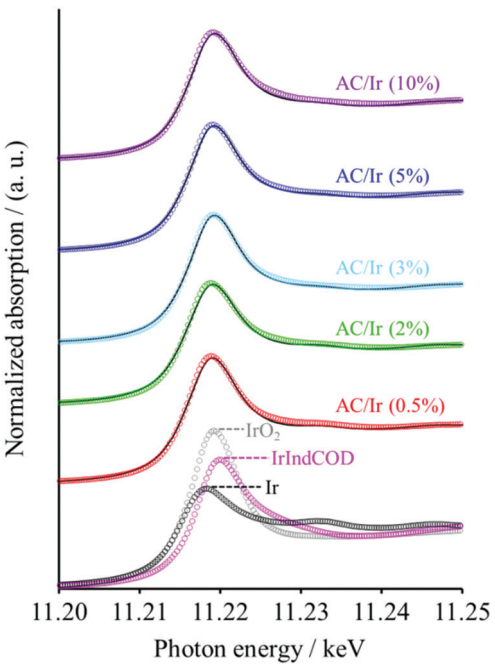

Fig. 4 XANES spectra of the samples. Solid lines correspond to the fitting results.

Table 1 Fitting results of the XANES spectra for the AC/Ir samples

	Molar ratio			
Total Ir content (wt%)	IrIndCOD	IrO_2	Ir	*R*-Factor
0.5	0.054 ± 0.024	0.464 ± 0.012	0.482 ± 0.012	0.0037
2	0.143 ± 0.022	0.331 ± 0.010	0.527 ± 0.010	0.0030
3	0.247 ± 0.020	0.410 ± 0.008	0.343 ± 0.008	0.0017
5	0.235 ± 0.020	0.382 ± 0.008	0.383 ± 0.008	0.0017
10	0.281 ± 0.024	0.380 ± 0.012	0.338 ± 0.012	0.0037

the number of nanoparticles with sizes of ~4 nm by simply increasing the heat treatment duration from 3 to 24 h or the heat treatment temperature from 400 to 500 °C for AC/IrIndCOD (10%) (Fig. S3 and S4, ESI†). The optimization for completely decomposing the adsorbed IrIndCOD for each sample is beyond the scope of the current study. The purpose of this study was to focus on the synthesis and structural analysis of the Ir nanoparticles below the pore size of AC by taking advantage of the pore confinement.

The remaining concern is the porosity of the AC/Ir samples necessary for the accessibility of substrates to the surface of the Ir nanoparticles within the AC pores when they are used as catalysts. The nitrogen adsorption/desorption measurement of the AC/Ir samples demonstrated that AC/Ir (10%) had a surface area of as high as 2310 $m^2\ g^{-1}$ and micro- and mesopore volumes of 0.75 and 0.43 $cm^3\ g^{-1}$, respectively (Table S1, ESI†). The other AC/Ir samples have larger surface areas and pore volumes than AC/Ir (10%) (for details, see the ESI†). Therefore, such large surface areas and pore volumes of the AC/Ir samples enable the access of substrates to the Ir nanoparticles when they are used as catalysts. In addition, the pore size distributions of the AC/Ir samples revealed that both micro- and mesopore volumes decreased by the Ir loading (Fig. S1, ESI†), indicating that Ir nanoparticles exist not only in the micropores but also in the mesopores, irrespective of the amount of Ir.

The proposed dry chemical method is obviously not limited to Ir metal nanoparticle synthesis and should be applicable to make other metal nanoparticles by selecting appropriate organometallic complexes and porous carbon supports. The size of the metal nanoparticles can be adjusted by using AC with appropriate pore sizes, and attention should be paid not to overlook the remaining complexes. Our XANES analyses identified the remaining metal precursor after the synthesis for high mass loading samples, indicating that XANES can be used for identifying the remaining precursors. This method would be desirable to systematically synthesize the nanoparticles without the undesirable formation of nanoparticles larger than the pore size of porous carbons and to discuss the correlation between the particle sizes and their performances as electrocatalysts, for example.

In summary, Ir nanoparticles with sizes less than the pore sizes of AC were finely dispersed over the whole AC particles *via* the dry chemical method. Undecomposed organometallic complexes in AC cannot be identified by TEM imaging and XRD analyses, while X-ray absorption analysis provided the information on the state of the supported Ir. This methodology can provide facile synthesis of the metal nanoparticles with sizes less than the pore sizes of porous carbons, by using appropriate organometallic complexes and porous carbons. The proposed dry chemical method is expected to be a facile method for optimizing the performances as electrocatalysts and other devices.

Conflicts of interest

There are no conflicts to declare.

Acknowledgements

This work was supported by JSPS KAKENHI Grant Number 17K06034.

Notes and references

1 K. Judai, S. Abbet, A. S. Wörz, U. Heiz and C. R. Henry, *J. Am. Chem. Soc.*, 2004, **126**, 2732–2737.
2 A. A. Herzing, C. J. Kiely, A. F. Carley, P. Landon and G. J. Hutchings, *Science*, 2008, **321**, 1331–1335.
3 S. Vajda, M. J. Pellin, J. P. Greeley, C. L. Marshall, L. A. Curtiss, G. A. Ballentine, J. W. Elam, S. Catillon-Mucherie, P. C. Redfern, F. Mehmood and P. Zapol, *Nat. Mater.*, 2009, **8**, 213–216.
4 A. Beniya and S. Higashi, *Nat. Catal.*, 2019, **2**, 590–602.
5 Y. Holade, E. N. Sahin, K. Servat, W. T. Napporn and B. K. Kokoh, *Catalysts*, 2015, **5**, 310–348.
6 F. Raimondi, G. G. Scherer, R. Kötz and A. Wokaun, *Angew. Chem., Int. Ed.*, 2005, **44**, 2190–2209.
7 B. Fang, N. K. Chaudhari, M.-S. Kim, J. H. Kim and J.-S. Yu, *J. Am. Chem. Soc.*, 2009, **131**, 15330–15338.
8 H. W. Kroto, J. R. Heath, S. C. O'Brien, R. F. Curl and R. E. Smalley, *Nature*, 1985, **318**, 162–163.
9 S. Iijima, *Nature*, 1991, **354**, 56–58.
10 S. Iijima and T. Ichihashi, *Nature*, 1993, **363**, 603–605.
11 K. S. Novoselov, A. K. Geim, S. V. Morozov, D. Jiang, Y. Zhang, S. V. Dubonos, I. V. Grigorieva and A. A. Firsov, *Science*, 2004, **306**, 666–669.
12 D. Salinas-Torres, J. M. Sieben, D. Lozano-Castello, E. Morallón, M. Burghammer, C. Riekel and D. Cazorla-Amorós, *Carbon*, 2012, **50**, 1051–1056.
13 D. Salinas-Torres, J. M. Sieben, D. Lozano-Castelló, D. Cazorla-Amorós and E. Morallón, *Electrochim. Acta*, 2013, **89**, 326–333.

14 H. Itoi, S. Hayashi, H. Matsufusa and Y. Ohzawa, *Chem. Commun.*, 2017, **53**, 3201–3204.
15 H. Itoi, S. Maki, T. Ninomiya, H. Hasegawa, H. Matsufusa, S. Hayashi, H. Iwata and Y. Ohzawa, *Nanoscale*, 2018, **10**, 9760–9772.
16 H. Itoi, K. Shimomura, H. Hasegawa, N. Nomura, Y. Ohta, H. Iwata, Y. Hoshikawa and Y. Ohzawa, *Adv. Mater. Interfaces*, 2019, **6**, 1801799.
17 C. D. Saquing, T.-T. Cheng, M. Aindow and C. Erkey, *J. Phys. Chem. B*, 2004, **108**, 7716–7722.
18 C. Galeano, J. C. Meier, V. Peinecke, H. Bongard, I. Katsounaros, A. A. Topalov, A. Lu, K. J. J. Mayrhofer and F. Schüth, *J. Am. Chem. Soc.*, 2012, **134**, 20457–20465.
19 S. Mayavan, J.-B. Sim and S.-M. Choi, *J. Mater. Chem.*, 2012, **22**, 6953–6958.
20 H. Itoi, H. Nishihara, S. Kobayashi, S. Ittisanronnachai, T. Ishii, R. Berenguer, M. Ito, D. Matsumura and T. Kyotani, *J. Phys. Chem. C*, 2017, **121**, 7892–7902.
21 H. Itoi, Y. Yasue, K. Suda, S. Katoh, H. Hasegawa, S. Hayashi, M. Mitsuoka, H. Iwata and Y. Ohzawa, *ACS Sustainable Chem. Eng.*, 2017, **5**, 556–562.
22 H. Itoi, H. Hasegawa, H. Iwata and Y. Ohzawa, *Sustainable Energy Fuels*, 2018, **2**, 558–565.
23 H. Nishihara, H. Fujimoto, H. Itoi, K. Nomura, H. Tanaka, M. T. Miyahara, P. A. Bonnaud, R. Miura, A. Suzuki, N. Miyamoto, N. Hatakeyama, A. Miyamoto, K. Ikeda, T. Otomo and T. Kyotani, *Carbon*, 2018, **129**, 854–862.
24 Y. F. Li, R. Hatakeyama, T. Kaneko, T. Izumida, T. Okada and T. Kato, *Nanotechnology*, 2006, **17**, 4143–4147.
25 L.-J. Li, A. N. Khlobystov, J. G. Wiltshire, G. A. D. Briggs and R. J. Nicholas, *Nat. Mater.*, 2005, **4**, 481–485.
26 H. Kobayashi, M. Yamauchi and H. Kitagawa, *J. Am. Chem. Soc.*, 2012, **134**, 6893–6895.
27 H. Nishihara, F. Ohtake, A. Castro-Muniz, H. Itoi, M. Ito, Y. Hayasaka, J. Maruyama, J. N. Kondo, R. Osuga and T. Kyotani, *J. Mater. Chem. A*, 2018, **6**, 12523–12531.
28 H. Itoi, H. Nishihara, T. Kogure and T. Kyotani, *J. Am. Chem. Soc.*, 2011, **133**, 1165–1167.
29 S. Kelly, R. Ingalls, F. Wang, B. Ravel and D. Haskel, *Phys. Rev. B: Condens. Matter Mater. Phys.*, 1998, **57**, 7543–7550.
30 J. W. Sobczak, E. Sobczak, A. Drelinkiewicz, M. Hasik and E. Wenda, *J. Alloys Compd.*, 2004, **362**, 162–166.
31 M. Takaoka, A. Shiono, K. Nishimura, T. Yamamoto, T. Uruga, N. Takeda, T. Tanaka, K. Oshita, T. Matsumoto and H. Harada, *Environ. Sci. Technol.*, 2005, **39**, 5878–5884.